THE JOURNAL OF PHYSICAL CHEMISTRY C

Article

Cite This: J. Phys. Chem. C 2018, 122, 29051−29061

pubs.acs.org/JPCC

New Insights into the Growth Mechanism of Ultrathin Au Nanowires from Combined in Situ EXAFS and SAXS Studies

Fernando Pschunder,[†] Julieta Puig,[‡] Lisandro J. Giovanetti,[†] Cristián Huck-Iriart,[†,§] Félix G. Requejo,[†] David Buceta,[∥] Cristina E. Hoppe,*[,‡] and José M. Ramallo-López*[,†]

[†]INIFTA, UNLP-CONICET, Diagonal 113 y 64, CP 1900 La Plata, Argentina

[‡]INTEMA, UNMDP-CONICET, Av. Juan B. Justo 4302, B7608FDQ Mar del Plata, Argentina

[§]Escuela de Ciencia y Tecnología, Universidad Nacional de San Martín (UNSAM), Campus Miguelete, 25 de Mayo y Francia, 1650 San Martín, Provincia de Buenos Aires, Argentina

[∥]Physical Chemistry Department, Faculty of Chemistry, and NANOMAG Laboratory, Research Technological Institute, University of Santiago de Compostela, E-15782 Santiago de Compostela, Spain

Supporting Information

ABSTRACT: The synthesis of Au nanowires (NWs) in hexane solution of $HAuCl_4 \cdot 3H_2O$, oleylamine and triisopropylsilane at room temperature was "in situ" monitored by means of X-ray absorption fine structure spectroscopies and small-angle X-ray scattering to determine, under identical synthesis conditions, both the changes in the oxidation state of gold atoms and the evolution of the size and shape of the objects involved in the formation of Au NWs. We propose a multistage process for the formation of the NWs: first, Au(III) atoms form a planar-square geometry complex that is continuously reduced to give Au(I) disk-like structures with diameters bigger than that of the final NWs. In a second stage, characteristic length/thickness ratio of these disk-like objects increases to form cylinders, presumably through aurophilic interactions between Au(I) centers and stacking of the disks. When most of the Au atoms have been reduced to Au(I), the reduction to Au(0) begins (third stage), and the NWs grow to form an hexagonal arrangement, separated by a bilayer of oleylamine molecules (fourth stage). Finally, a slow reduction leads the reaction to the final product, formed by bundles of long, ultrathin Au NWs.

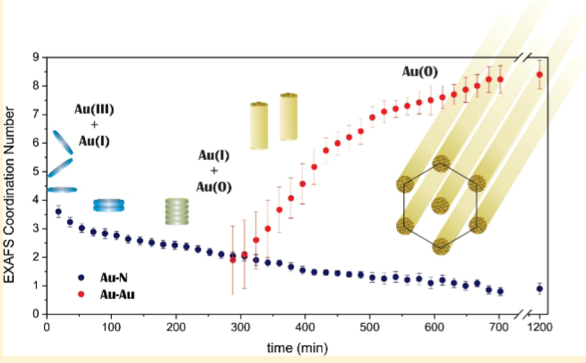

1. INTRODUCTION

Single-crystalline, ultrathin gold nanowires (Au NWs) have attracted the attention of many research groups, especially since the first works reporting their synthesis by wet chemistry.[1−6] This advance has been a fundamental step that has given the possibility of obtaining Au NWs by straightforward procedures with high yields and opened the way to a myriad of potential technological applications based on the development of electrical sensors,[7,8] fuel cell anodes,[9] elastic coiled springs,[10,11] transparent electrodes,[12,13] etc. The unique one-dimensional (1D) features of Au NWs, as well as their ultralow diameter, confer them remarkable physical properties (e.g., disappearance of surface plasmon and appearance of interband transitions, changes in conductivity, etc.), paving the way to new applications in nanoelectronics. Demonstration of their self-assembly on transmission electron microscopy (TEM) carbon grids has also showed their potential for the design of new artificial nanomaterials.[14]

Several strategies have been followed to synthesize Au NWs, most of them based on the chemical methods first proposed between 2007 and 2009 by different groups.[1−6] The approach was mainly based on the reduction of a gold salt ($HAuCl_4$ or AuCl) in pure oleylamine (OAm)[4] or in a OAm solution containing an additional reducing agent.[1] Although OAm can be used alone as both stabilizing and reducing agent, higher yields of gold nanowires were obtained in the presence of an external reducing molecule like triisopropylsilane (TIPS).[15]

To take advantage of the singular properties of these NWs, the mechanism behind their formation has to be solved. Without a detailed knowledge of the steps that occur during the synthesis process of NWs and because of the complex interplay between variables involved, no accurate control on the yield, diameter tuning, chemical composition, capping thickness, etc. can be achieved. More importantly, realistic possibilities of scaling-up for their use at industrial scale cannot be envisaged without this basic knowledge. The understanding of the processes involved during the growth becomes

Received: October 26, 2018
Revised: November 23, 2018
Published: November 28, 2018

DOI: 10.1021/acs.jpcc.8b10449
J. Phys. Chem. C 2018, 122, 29051−29061

fundamental for technological applications of ultrathin Au NWs.

Since the first reports of the synthesis, different mechanisms have been proposed to explain the anisotropic growth and gain control on the different variables that regulate their production. A complete picture of the synthesis process should include information about the reduction pathway of Au species along the synthesis, the role of OAm in the formation of 1D objects, and the evolution of the morphology leading to the final state of the wires. Halder et al. proposed an oriented attachment of small seeds formed by aging of an Au(I) precursor to explain the anisotropic growth of these wires.[1] One year later, Xia's group proposed a reduction mechanism assisted by aurophilic interactions between Au(I) complexes forming polymeric strands with oleylamine.[2] Wang et al.[5] and Pazos-Pérez et al.[6] invoked a micellar growth based on the formation of small crystals inside reverse micelles, formed by the presence of oleylamine. More recently, Loubat et al., on the basis of the small-angle X-ray scattering (SAXS) experiments and preliminary density functional theory calculations, proposed the existence of a "zip" mechanism and ruled out the possibility of oriented attachment.[16,17]

Hence, the growth mechanism of Au NWs synthesis is still a matter of debate. Major challenges have been related to the experimental complexity involving realistic determination of the evolution of the crystals into 1D objects and the lack of conclusive evidence about the reduction pathway of Au species along the reaction. Regarding this last issue, several authors have already proposed a two-step reduction process going from Au(III) to Au(I) and then to Au(0),[2,4,17,18] mainly based on X-ray photoelectron spectroscopy and TEM characterizations. Both techniques involve the evaporation of solvent and ultrahigh-vacuum conditions. Under these circumstances, both the TEM electrons[19,20] and X-ray[21,22] beams can produce radiation damage and sample heating that can lead to cleavage or desorption of adsorbates, changes in the oxidation state of the metal atoms, and particle sintering. To avoid misleading interpretations, "in situ" characterization becomes essential for univocally determining the oxidation state changes during the process under realistic conditions.

In this work, we performed a combined in situ characterization, through X-ray absorption fine structure spectroscopy (X-ray absorption near edge structure (XANES) and extended X-ray absorption fine structure (EXAFS)) and small-angle X-ray scattering (SAXS), along with the complete reaction. The idea behind this approach was to determine, under identical synthesis conditions, both the changes in the oxidation state of gold and the evolution of size and shape of the objects that give place to the formation of Au NWs. UV−vis spectroscopy and TEM were also used as supporting techniques.

2. EXPERIMENTAL SECTION

2.1. Au NWs Synthesis. Au NWs were synthesized at room temperature using a modification of the procedure described by Loubat et al.[17] This synthesis is based on the original work by Feng et al.[15] that uses hexane as a solvent and triisopropylsilane (TIPS) as an external reducing agent. Briefly, 3.0 mg of $HAuCl_4 \cdot 3H_2O$ (49 wt % metal basis) was dissolved in a solution containing 0.1 mL of oleylamine (OAm, technical grade, 70%) in 0.5 mL of hexane P.A. Immediately after the dissolution of the metallic salt, 0.15 mL of TIPS (98%) was added. The solution was kept at room temperature (22 °C) without stirring. For some selected experiments, the same procedure was followed in the absence of TIPS. Also, the synthesis was carried out at 40 °C for comparative purposes. All the reagents and solvents were obtained from Aldrich and used as received.

2.2. Small-Angle X-ray Scattering (SAXS). SAXS measurements were performed using a XEUSS 1.0 (from XENOCS) equipment with a two-dimensional photon-counting pixel X-ray detector Pilatus 100k (DECTRIS, Switzerland). The scattering intensity, $I(q)$, was recorded in the range of the momentum transfer $0.04 < q < 6$ nm^{-1}, where $q = 4\pi/\lambda \sin(\theta)$, 2θ is the scattering angle, and $\lambda = 0.15419$ nm is the weighted average of the X-ray wavelength of the Cu Kα_{12} emission lines. Due to the small beam size at the sample (1 mm × 1 mm), smearing effects were not taken into account. Reaction took place at room temperature within an in-house sample holder suitable for organic liquids, employing Kapton windows. Each SAXS pattern was taken every 10 min during 16 h. The reported data were corrected for the solvent scattering and processed using standard procedures.

2.3. X-ray Absorption Fine Structure (XAFS) Spectroscopy. X-ray absorption spectroscopy measurements experiments were performed at the XAFS2 beamline at the Laboratorio Nacional de Luz Sincrotron (LNLS), Campinas, Brazil. The EXAFS spectra of the Au L_3 (11919 eV) edge were recorded at room temperature using a Si(111) channel-cut monochromator. All the experiments were done in transmission mode with three ion chambers as detectors with gas mixture optimized to improve the measured signal. Third ionization chamber was used to measure the Au metallic reference simultaneously with the sample for energy calibration. The sample was placed in a Teflon liquid cell with Kapton windows. Preliminary XANES studies were performed using a RIGAKU R-XAS Looper Spectrometer.

The XAFS spectra were collected in the XANES and EXAFS regions every 18 min. The EXAFS data were extracted from the measured absorption spectra by standard methods using the ATHENA software, which is part of the IFFEFIT package.[23] Fourier transformation was calculated using the Hanning filtering function. The EXAFS modeling was carried out using the ARTEMIS program from IFFEFIT package. The structural parameters (coordination numbers, bond lengths, and their mean squared disorders) were obtained by a nonlinear least-squares fit of the EXAFS signal in R. The theoretical scattering path amplitudes and phase shifts for all the paths used in the fits were calculated using the FEFF code.[24] The k-range was set from 2 to 11 Å^{-1} and the Fourier transforms were fitted in different regions. The passive reduction factor S_0^2 was restrained to a value of 0.92. This value was obtained from fitting the EXAFS spectrum of a metallic face-centered cubic Au foil and by constraining the coordination number to the value of 12.

2.4. Transmission Electron Microscopy (TEM). TEM and high-resolution TEM (HRTEM) images were obtained in a Field Emission Gun Transmission Electron Microscope, JEOL JEM2010F FEG-TEM operating at 200 kV. The samples were obtained by dropping 5 μL of the reaction dispersion (diluted at 1:10 ratio with hexane) on TEM grids coated with carbon and a Formvar film.

2.5. UV−vis Spectroscopy. The UV−vis spectra were taken in situ during the synthesis at room temperature using a diode-array spectrophotometer (Agilent 8453) with a Peltier accessory. Cells with two different optical paths (1 and 10 mm) were used depending on the stage of the reaction to

DOI: 10.1021/acs.jpcc.8b10449
J. Phys. Chem. C 2018, 122, 29051−29061

maximize the sensitivity, whereas avoiding the saturation of the detector.

2.6. Atomic Force Microscopy (AFM). Atomic force microscopy images of the objects formed during the first minutes of the reaction ($t \leq 15$ min) were obtained using a Multimode microscope and Nanoscope V control unit from Veeco Instruments. Images were obtained in contact mode at a scan rate of 1.0−1.2 Hz. A contact sharpened silicon nitride probe (NP-10, Veeco) with tip radius of 15−20 nm and spring constants with characteristic values of 0.06 N/m was used. The samples were prepared by dispensing a few drops of the solution on a mica substrate and letting them dry.

3. RESULTS

3.1. Synthesis. The synthesis was carried out under similar (but not identical) conditions to those previously reported in the literature.[15,17] A more concentrated initial solution of gold was used compared to that used in the synthesis method developed by Feng et al.[15] (5 times less hexane as solvent) and the reaction was kept at room temperature, in contrast to the higher temperature (40 °C) used by Loubat et al.[17] Hence, the first step of this work consisted in analyzing the final product of the reaction to determine how these conditions affected the production and yield of ultrathin Au NWs.

The TEM images obtained after 12 h of synthesis at room temperature show that the final product of the reaction consists of single-crystalline Au NWs of about 1.7 nm diameter and several micrometers length (Figure 1a,b). The UV−vis spectrum shows a peak at around 490 nm (indicated by the arrow), assigned to the formation of quantized electronic structures, and no significant absorption associated with the presence of plasmonic resonances, which is in agreement with the low diameter of the wires and an undetectable contamination of subproducts as spheres or rods[25] (Figure 1c). An almost identical spectrum was obtained when the reaction was performed at 40 °C, indicating that the nature of the products does not significantly change in this temperature range. Small differences could be attributed to minor changes in length distribution of the wires and slight differences in the concentration of the initial reactive solution.

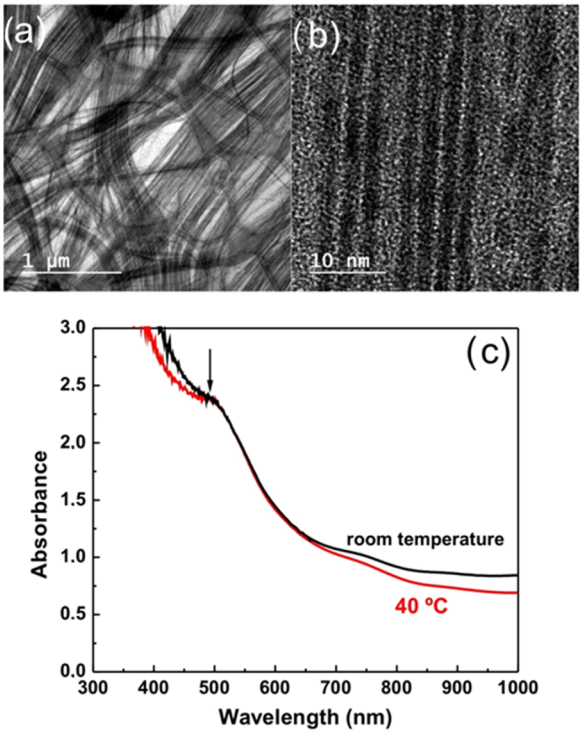

Figure 1. (a) TEM micrograph of the product obtained after 12 h of reaction at room temperature. (b) HRTEM micrograph showing the single-crystalline character of the obtained Au NWs. (c) UV−vis spectra after 12 h of reaction at room temperature (black curve) and 40 °C (red curve).

3.2. UV−vis Spectrophotometry. Once the selected experimental conditions were validated, a spectrophotometric analysis of the reaction was carried out. Synthesis starts with the addition of TIPS to a solution of $HAuCl_4$ and OAm in hexane. However, some changes are produced in the system even in the absence of TIPS due to the presence of OAm that acts as both coordinating ligand and soft reducing agent. This can be clearly seen by visual inspection and using UV−vis spectrophotometry. Interestingly, the initial curve is characterized by a band centered at about 375 nm that decreases slowly with time even in the absence of TIPS (Figure 2a). The decrease in this absorption peak at 375 nm occurs continuously during the first 60 min of the reaction to give a slightly yellow solution. This color transition has been previously reported and attributed to the reduction of the Au(III) complex to Au(I) species.[26] Figure 2b shows how the absorption spectrum changes when TIPS is added to the reaction. Again, the initial curve ($t = 0$) can be assigned to the orange complex of Au(III) and the absorption peak at 375 nm decreases during the first 60 min, at the same rate as in the absence of TIPS, presumably by the reduction of Au(III) to Au(I). From this moment on, the curve changes with respect to the sample without TIPS, decreasing in intensity until 135 min. However, no clear evidence of the formation of Au NWS or other form of Au(0) structures appears until 230 min after the addition of TIPS, when a small peak centered around 490 nm appears and can be associated to the formation of quantized electronic structures compatible with very small metallic nanostructures[25] (Figure 2c).

Changes during the reaction can be better observed by analyzing the evolution of the absorbance at 375 and 490 nm as a function of time (normalized with respect to the initial absorbance at the selected wavelength). Figure 2d shows that, in the first hour of reaction, absorbance at 375 nm changes almost at the same rate both in the absence and the presence of TIPS. These results are consistent with the XANES results, which show a similar decrease in the white line intensity at the Au L_3 edge after 60 min of reaction in both cases (see Supporting Information, Figure S5). This behavior indicates that the first stages of reduction of Au(III) to Au(I) would not be influenced by the presence of this reducing agent. However, after this time, the system with TIPS clearly changes respect to the system without TIPS. Absorbance at 375 nm decreases up to 135 min and then remains constant until about 160 min, moment in which the band at 490 nm starts to increase. Presumably, the formation of Au(0) starts at this time, becoming clearly visible at about 230 min. From this moment on, the absorbance at 490 nm increases almost linearly with time.

3.3. TEM Analysis. The TEM micrographs were obtained at the beginning and after 10 h of reaction. It is important to recall that this technique is not able to reproduce with precision what is happening in the reaction medium. Being an "ex situ" technique and due to the effects of solvent

DOI: 10.1021/acs.jpcc.8b10449
J. Phys. Chem. C 2018, 122, 29051−29061

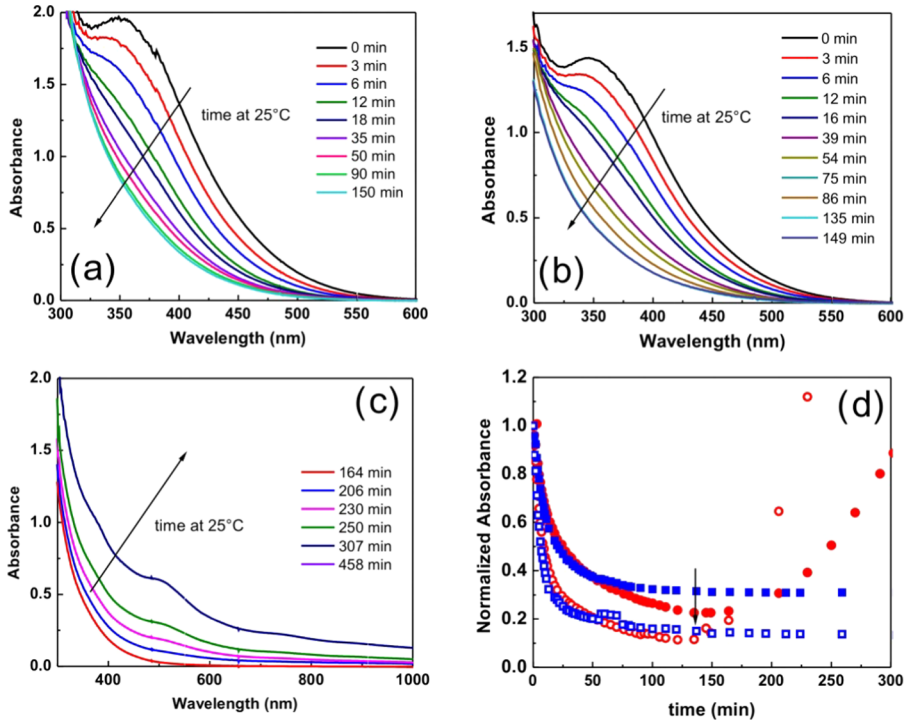

Figure 2. Evolution of the UV−vis spectra of a sample of $HAuCl_4$/OAm/hexane in the (a) absence and (b) presence of TIPS. (c) Evolution of the curves at longer reaction times in the presence of TIPS. (d) Normalized absorbance as a function of time in the presence (red symbols) and absence (blue symbols) of TIPS at 375 nm (filled symbols) and 490 nm (open symbols).

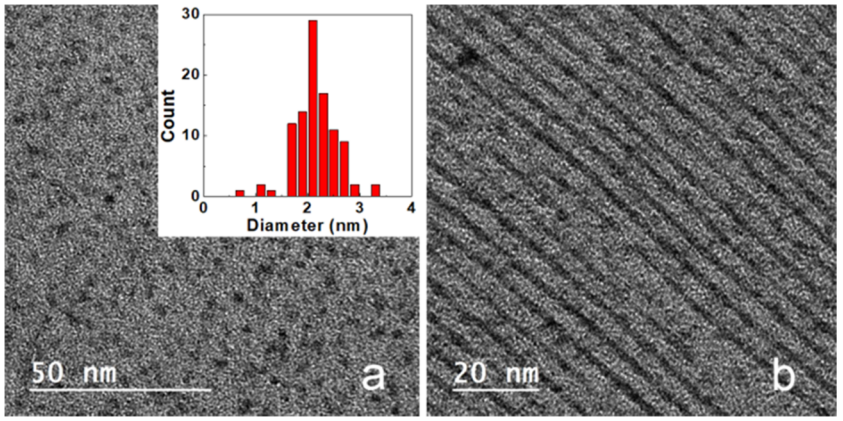

Figure 3. TEM images obtained at (a) 0 min and (b) 600 min of reaction. Inset in (a) shows the size distribution of the objects.

evaporation, interaction with the substrate and, most importantly, the possible damage produced by the interaction with the electron beam, the results should be considered only as an additional tool for interpretation. However, even without precision or details, some estimation regarding the shape of the objects formed at the beginning of the reaction can still be done. Figure 3 shows the TEM micrographs obtained at the beginning and after 600 min of reaction. The samples were extracted from the reaction medium, diluted in hexane, and deposited on a TEM grid before imaging. Figure 3a shows the presence of a narrow distribution of objects with a very low electronic contrast and a mean size of approximately 2.2 nm. A poor definition and a low contrast of these structures are incompatible with the presence of spherical, metallic objects. Only a few of them, appearing darker in the TEM grid, could be identified as metallic spherical particles, which were probably formed during the imaging process by the interaction with the electron beam. As we will show later, no metallic object is present in the reaction medium during the first hours of reaction. After 600 min, the reaction is complete and the observed structures are long, single-crystalline nanowires of about 1.7 nm diameter (Figure 3b).

3.4. In Situ SAXS Analysis. In situ SAXS studies of the formation and growth of Au NWs was carried out. The SAXS curves as a function of the transferred momentum (q) taken every 10 min are shown in Figure 4.

Evolution of the curves occurs through several different stages. The first one (up to 160 min) is characterized by SAXS curves with an almost constant shape and intensity. The choice of a model that adequately fits the experimental curves at the first part was based on the particle distance distribution function $p(R)$ conversion, employing the GNOM software,[27] of the initial experimental pattern (Figure 5). The SAXS curve, which characterizes the initial complex was obtained by

DOI: 10.1021/acs.jpcc.8b10449
J. Phys. Chem. C 2018, 122, 29051−29061

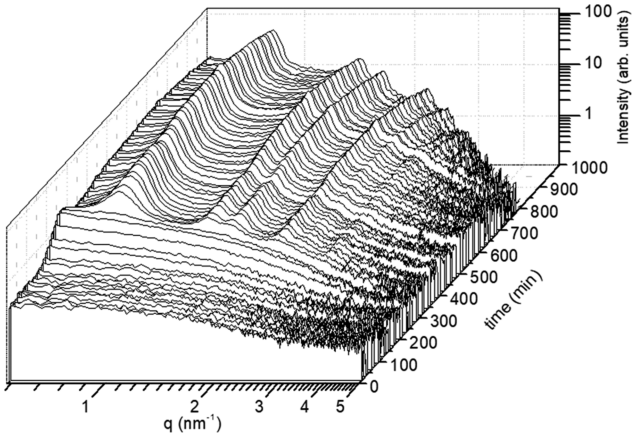

Figure 4. In situ SAXS patterns of the reactive sample taken every 10 min during 16 h.

averaging six exposition patterns taken during 10 min each (without TIPS). The shape of the $p(R)$ observed in Figure 5b does not seem to be compatible with that expected for a set of polydisperse spheres with a size dispersion and an average size like the one that can be observed in the TEM images (see Figure S1, Supporting Information). The analysis of these curves indicates that the shape of the objects present at the beginning of the reaction is not compatible with spheres. Instead, the experimental data can be fitted by considering randomly oriented cylinders with negligible correlation (see the Supporting Information). The cylinder diameter, defined as $D = 2R$, has a constant value of about 2.6 nm and a length, L, smaller than D at this stage (Figure 6a,b respectively), suggesting they can be best considered as disk-like objects. A detailed description of the fitting function is shown in the Supporting Information. To validate this particle model used for the SAXS analysis, atomic force microscope (AFM) images on contact mode of the initial particles supported on a mica substrate were obtained (Figure S2, Supporting Information). An analysis of the height distribution of this sample showed the presence of flat particles with height of 0.5 ± 0.1 nm (see the Supporting Information), compatible with anisotropic disk-like structures. As previously mentioned, the SAXS patterns show only slight changes during this time, indicating that the morphology is preserved during the first stage of the synthesis. However, some subtle differences in the curves indicate that the characteristic length/thickness of the objects, L, increased at longer times of the stage. Between 60 and 120 min, L increases from about 0.3 to 1−1.25 nm, indicating the initiation of a second step of aggregation: stacking of the disks to form cylinders (inset in Figure 6b).

After 160 min, curves start to evolve, showing a change to objects of bigger sizes evidenced by the increase from 0 to 1 of the slope (in log−log scale) within the small-angle regions (Figure 6c). This change is in agreement with the growth of a one-dimensional (1D) object, compatible with the appearance of nanowires. At the beginning of this process, there is a visible and sudden shift in the middle-angle region curvature to wider angles due to a shrinkage in the cylinder diameter to 1.6 nm.

After 250 min of reaction, correlation between objects is reflected by the appearance of six peaks in well-defined positions in the SAXS curves, indicating the presence of long range positional order (Figure 7). The positions of the peaks in the reciprocal space relative to the position of the first peak are $1:\sqrt{3}:\sqrt{4}:\sqrt{7}:\sqrt{9}:\sqrt{13}$, characterizing a two-dimensional hexagonal network in the plane normal to the nanowires. This effect was taken into account by the inclusion of a structure factor in the cylindrical model (described in the Supporting Information).

The lattice parameter of this hexagonal arrangement, "a", was calculated from the distance between the reflections: $d(hk) = a/(h^2 + k^2 + hk)$ and gives an initial value of 9.4 nm, which immediately decreases to 9.0 nm and remains for more than 10 h around this value (Figure S3, Supporting Information). In addition, the fits show that the relative positions between the peaks do not change with time, indicating no modifications in the type of arrangement during the course of the reaction.

3.5. In Situ XAFS spectroscopy. To determine the local structure of the Au−oleylamine complexes present from the beginning of the reaction, the EXAFS experiments were performed in a liquid cell at the Au L_3-edge, using a sample obtained following the synthesis protocol described before but without the addition of TIPS. As shown by XANES at the Au L_3-edge, the complex is not stable in time, evolving quickly once the reagents are mixed (see XAFS section in the Supporting Information). For this reason, a quick measurement of only 10 min was done, with the drawback of having to sacrifice some statistics to obtain the spectrum of the initial state of the complex. Figure 8a shows the Fourier transform of the EXAFS spectrum and the corresponding fit proposing one

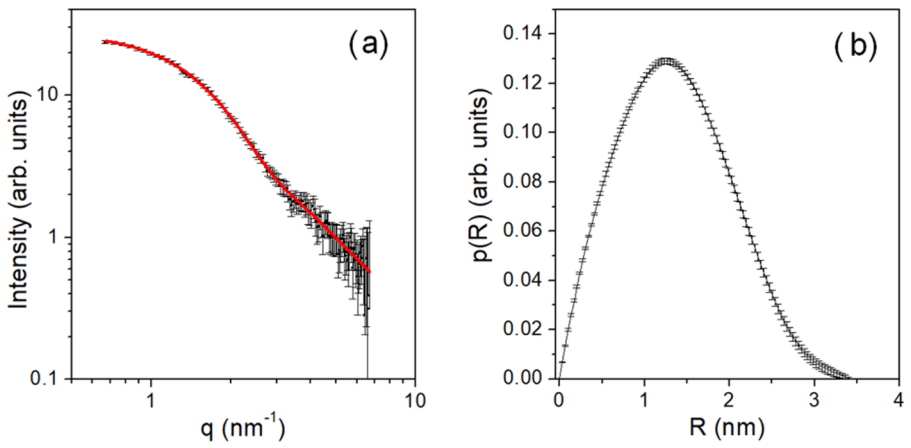

Figure 5. (a) SAXS pattern for the initial Au(III) complex (obtained in the absence of TIPS) and (b) $p(R)$ transformation.

DOI: 10.1021/acs.jpcc.8b10449
J. Phys. Chem. C 2018, 122, 29051−29061

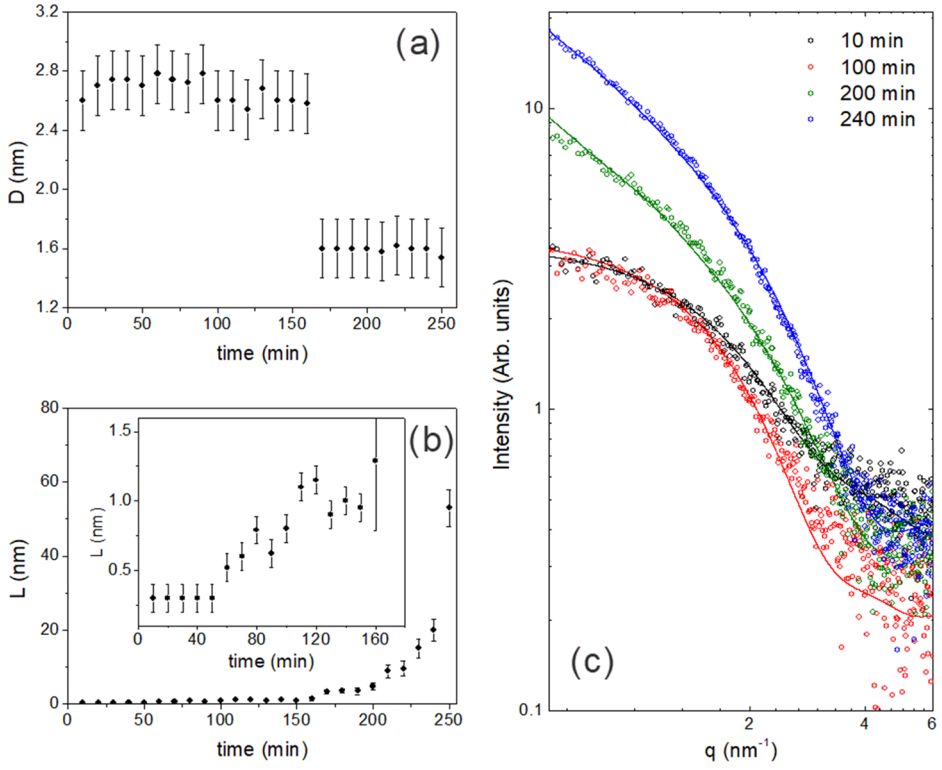

Figure 6. Evolution of (a) the diameter D and (b) length L of the objects present during the first 250 min of the reaction obtained from the analysis of SAXS data. The first 160 min were zoomed for a better view (inset). (c) SAXS patterns for Au NWs formation at different times before the appearance of correlation. The circles correspond to experimental data and the solid lines to the fitting obtained for the proposed model.

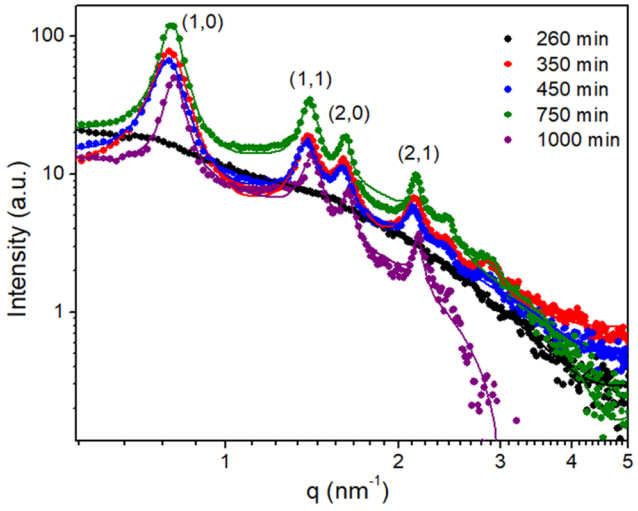

Figure 7. SAXS dispersion intensity obtained at several times after 250 min of reaction. The points correspond to the experimental data and the lines to the fits taking into account a form factor with contributions of cylinders and a structure factor of a hexagonal lattice.

shell of the possible light atoms bound to the gold atoms in the initial complex (N and Cl atoms). Although the coordination number of each type of atom cannot be univocally determined from these fits, a total coordination number of 3.9 ± 0.3 atoms at a distance of 2.04 ± 0.01 Å could be postulated at this very first moment of the reaction. These results are compatible with the presence of a square-planar Au(III) complex.[28]

Figure 8b shows the XANES spectra at the Au L_3-edge obtained during the whole reaction process. The decrease in the white line intensity is indicative of the reduction of the Au oxidation state. The appearance of bounces at 11 950 and 11 974 eV are characteristic of the reduction to Au(0) and the appearance of metallic entities (see Figure S4). A linear combination fit of XANES spectra was performed, using the Au−oleylamine complex spectrum (corresponding to Au(III)) and the last spectrum obtained after 20 h (corresponding to metallic gold) to consider a possible coexistence of two components with the oxidation states of Au(III) and Au(0). This approximation was not satisfactory, and the presence of a new component with a different oxidation state is necessary to improve the fitting substantially. Moreover, the final-state spectrum may not represent all the metallic states present during the NWs formation either, as it is well established that the XANES spectrum of the metallic nanostructures changes with the size and presence of capping molecules.[29]

In situ EXAFS experiments were also performed during the reaction. Figure 9a shows the Fourier transforms of the spectra taken every 18 min during 12 h of reaction. The spectra evolve from the one similar to that of the four-coordinated Au(III) complex to the final-state characteristic of metallic gold (although with a smaller amplitude). The intensity of the peak corresponding to a shell of light atoms decreases with time. After 280 min, new peaks appear at longer distances assigned to the building of an Au coordination shell due to the formation of metallic particles. The amplitude of these peaks increases with time, indicating the reduction of gold atoms and the growth of metallic particles.

To quantify the changes observed in the local structure around Au atoms, curve fittings to every spectrum were performed proposing two coordination shells: one of light atoms (represented by N atoms) and another one of Au atoms (Figure S6 and Table S1, Supporting Information). Reduction

DOI: 10.1021/acs.jpcc.8b10449
J. Phys. Chem. C 2018, 122, 29051−29061

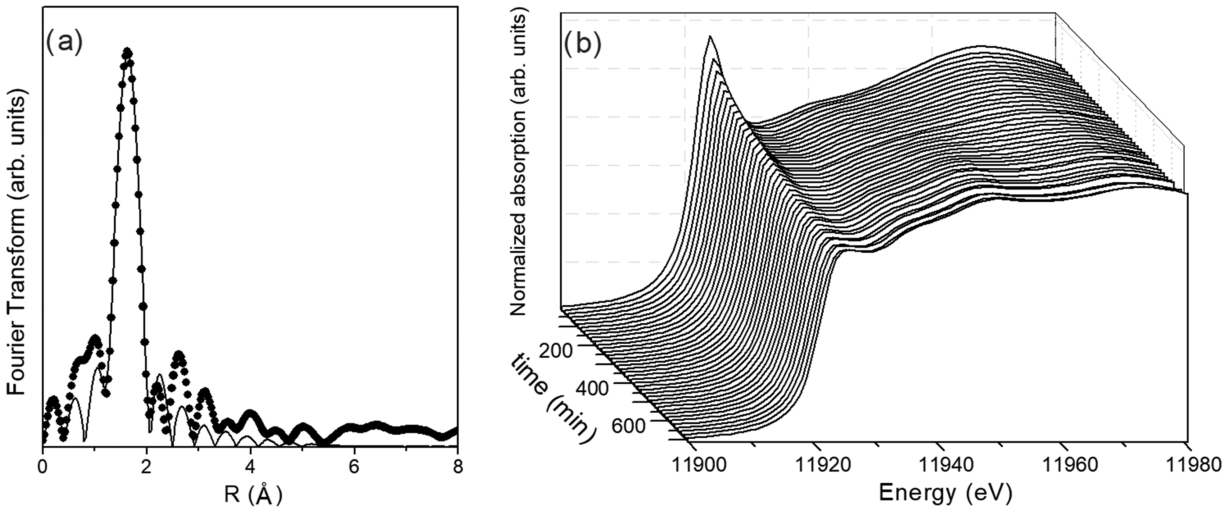

Figure 8. (a) Fourier transform of the EXAFS oscillation at the Au L_3-edge of the Au−oleylamine complex in hexane without TIPS (black circles) and the corresponding fit (solid line). (b) XANES spectra at the Au L_3-edge showing the evolution of the Au NWs over time.

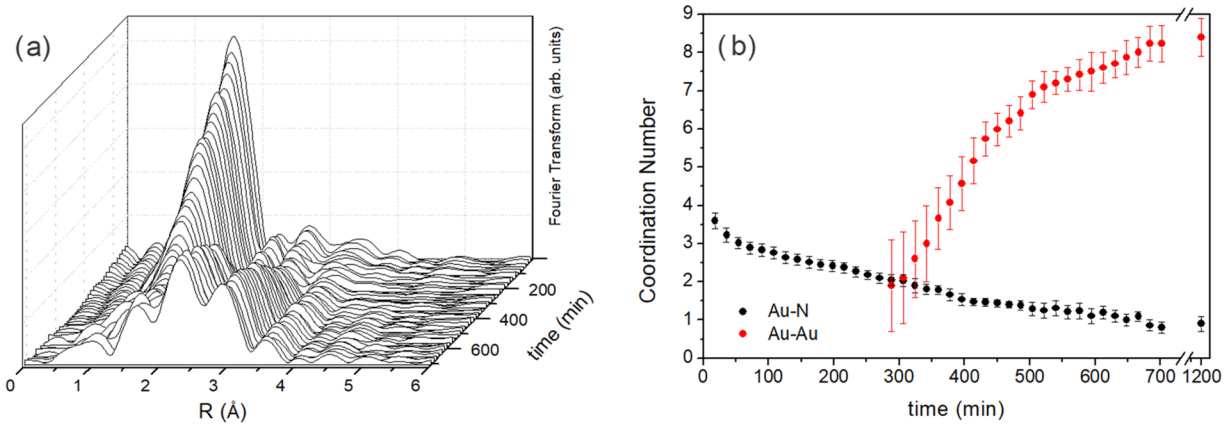

Figure 9. (a) Evolution over time of the Fourier transform of the EXAFS oscillations at the Au L_3-edge. (b) Evolution of the fitted average coordination numbers for Au atoms: black symbols correspond to coordination with light atoms; red symbols correspond to coordination with Au.

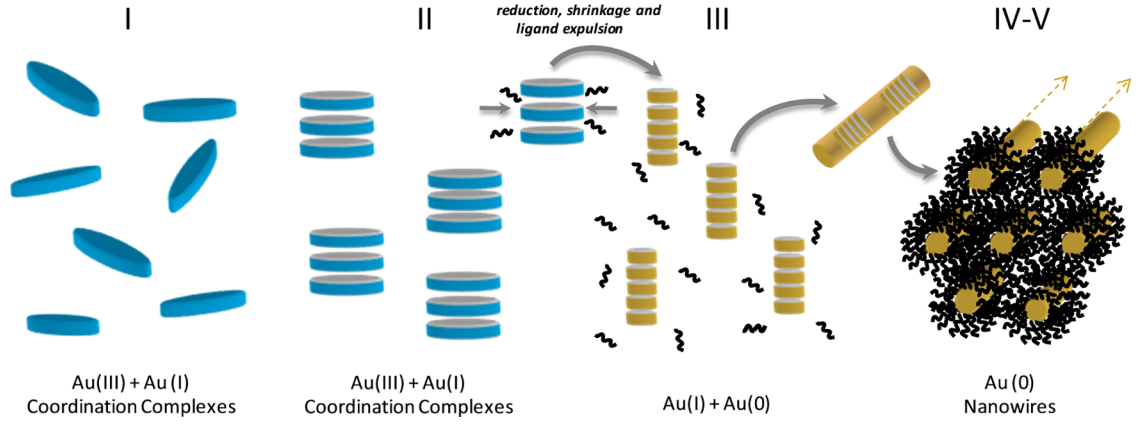

Figure 10. Schematic representation depicting the five stages of the proposed growth mechanism: in stage I, nonspherical, disk-like units are formed by coordination of oleylamine with Au(III) followed by partial reduction of Au(III) to Au(I). In stage II, these units are arranged to form cylindrical stacks that, by reduction of Au(I) to Au(0) and expulsion of ligands, suffer a diameter shrinkage with the formation of longer species (stage III). Joining of individual units takes place at this stage, along with stabilization of the formed nanostructures by the adsorption of OAm molecules on the metal surface. In stage IV, the formed wires are arranged in a hexagonal arrangement with a separation between nanostructures of about 7.3 nm, associated to the formation of a bilayer of OAm molecules. In stage V, Au−Au coordination number continues to increase at a lower speed as the length of the NWs grows.

of the oxidation state of Au should lead to a reduction in the Au average coordination number with light atoms. Hence, the average coordination numbers will give information on the oxidation state of Au atoms during the process. Figure 9b

DOI: 10.1021/acs.jpcc.8b10449
J. Phys. Chem. C 2018, 122, 29051−29061

shows the evolution over time of the fitted average coordination numbers for Au atoms.

The results of the fit of the first spectrum show an average coordination number with light atoms of 3.6 ± 0.2. For these fits, a shell of N atoms was proposed, but the presence of Cl atoms in this coordination shell cannot be ruled out. For this reason, this coordination number would represent the total coordination with light atoms (N and Cl atoms). A value between 2 and 4 is the result of the coexistence of both Au(III) and Au(I) species. The first 270 min of the reaction are characterized by a slow reduction in the coordination number from 3.6 to 2 (Figure 9b). This decrease is faster in the first 60 min of the process, in agreement with changes found by UV−vis spectrophotometry. After 270 min of reaction, the Au coordination number with light elements reaches a value close to 2, indicating that a high proportion of Au atoms have been reduced to Au(I). Shortly after that, a new coordination shell appears corresponding to Au(0) atoms, indicating the appearance of the first metallic species. From this moment on, the Au−Au coordination number grows continuously to reach a value of 8.3 after 720 min. Another EXAFS spectrum was acquired after 20 h of the beginning of the synthesis and the coordination numbers did not show significant changes from those obtained after 720 min of reaction.

4. DISCUSSION

Initial results show that Au NWs synthesis can be carried out at room temperature and at high concentrations without significant changes in the nature or yield of the reaction product. After 720 min of reaction (12 h), ultrathin Au NWs of 1.7 nm diameter are obtained in almost absence of spheres or rods (Figure 1). This result represents a significant finding, not only for application purposes but also for the elucidation of the mechanism of the formation of NWs, which constitutes still a matter of debate. Selected experimental conditions allow to follow the different stages during the process by using X-ray absorption spectroscopies and SAXS in situ measurements.

Analysis of the results obtained through different techniques allows to divide the synthesis process in five differentiated stages, as they are described below (see Figure 10).

4.1. Stage 1: 0−60 min of Reaction. $HAuCl_4$ is an Au(III) metallic precursor insoluble in hexane but soluble in the presence of OAm. Solubility of this salt in hexane is explained by the formation of a coordination complex characterized by a typical orange color. Although the nature of this complex cannot be completely clarified at this point, the nature of the ligands and the electronic configuration of Au(III) (d^8) points to a structure characterized by a planar-square geometry.[28] Spectrophotometric analysis (Figure 2) and EXAFS results (Figure 9b) show that this complex should be the main structure present at t = 0. However, both techniques also demonstrate that, in the presence or absence of TIPS (see Figure S5, Supporting Information), Au(III) complex is easily reduced to generate a linear Au(I) complex (slightly yellow), making it very difficult to find Au(III) species alone under the reaction conditions. Hence, these results would show that TIPS does not play a reducing effect in this first stage of the synthesis, which could be related to the steric effects precluding approximation or attack of this reagent to the Au(III) complex.

The structure of the Au(I) complex has been proposed as formed by an Au(I) center coordinating linearly to one chlorine atom and one OAm molecule. In this last case, two possibilities have been proposed for OAm coordination: by the nitrogen atom[2] or by the double bond of OAm[30] (Scheme 1).

Scheme 1. Proposed Coordination of OAm with Au(I)

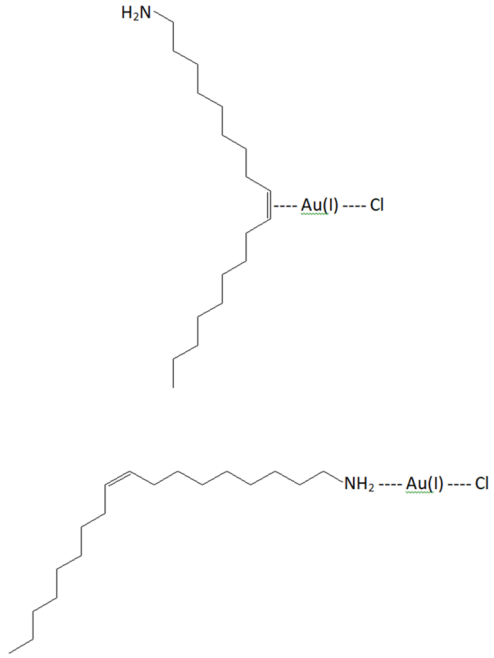

Analysis of the evolution of the average coordination number with light atoms obtained by EXAFS (Figure 9b) shows that in the first 60 min of the reaction, a fast decrease occurs from the initial value of around 4. An average coordination number between 2 and 4 suggests the simultaneous presence of complexes of Au(I) (coordination number of 2) and Au(III) (coordination number of 4). No evidences of Au−Au coordination are observed during this stage of the reaction.

As observed from the SAXS measurements (Figure 6a), the first 60 min of the reaction are characterized by the presence of objects with a diameter of about 2.6 nm (which is also in the range of sizes observed in the TEM micrographs, Figure 3a) and thickness of about 0.3−0.5 nm, with no evident structural changes (Figure 6b). These results point to the formation of disk-like structures by the aggregation of Au(I) and/or Au(III) complexes. The presence of anisotropic flat particles with a very homogeneous height at the beginning of the reaction was confirmed by AFM analysis (see the Supporting Information). A possible structure compatible with the observed sizes should include interactions in the plane and out of the plane between those complexes to form disks. Thickness of the disks (about 0.3 nm) is compatible with a possible interaction between two Au(I) centers, belonging to independent planar structures, via aurophilic interactions.[31] On the other hand, stabilization of planar structures of about 2.6 nm, formed by the gold complexes, could occur through interaction between chlorine and Au(I) atoms,[32] chlorine and NH_2 groups,[30] or hydrogen bonding between NH_2 groups, depending on the actual structure of the complex. Even aurophilic interactions between gold atoms located in the same plane could take place, without the detriment of the interactions occurring out of the plane.[31] Even more, they could be also formed by structures sharing both oxidation states (I and III). As it has been demonstrated,[31] the existence of structures presenting

DOI: 10.1021/acs.jpcc.8b10449
J. Phys. Chem. C 2018, 122, 29051−29061

aurophilic interactions between both types of gold centers is also possible.

In summary, elucidation of the interactions leading to aggregation and formation of these initial disk-like objects will require defining the structure of both complexes and their possible interactions in a more precise way, which is beyond the aim of this work. However, the main result of this part of the analysis can be summarized as follows: initial objects are not spherical (as proposed before by other authors[16]) but disk-like structures with a diameter of about 2.6 nm (bigger than the diameter of final NWs) and a thickness of about the distance between two gold atoms interacting through aurophilic interactions. More importantly, reduction from Au(III) to Au(I) takes place in the presence or the absence of TIPS, which would be indicating that this reagent does not play a role of a reducing agent in this stage of the synthesis. Although the reason for this behavior cannot be clarified at this point, it seems possible that it can be related to the steric effects avoiding the attack of TIPS to the square-planar Au(III) complex. On the contrary, oleylamine, which is in large excess with respect to the gold precursor, would be responsible for the reduction from Au(III) to Au(I) in this step of the reaction.

4.2. Stage 2: 60−160 min of Reaction. During this stage, SAXS measurements show an increase in length/thickness of the disk-like objects. Between 60 and 160 min, this value increases from about 0.3 nm to 1.00−1.25 nm (Figure 6b). This result could be indicating an aggregation process occurring through the interaction between Au(I) centers (stacking of the disks to form cylinders of longer length). Assuming aurophilic interactions between planar aggregates, this length would be associated with objects formed by 4−6 individual aggregates stacking to form a cylinder. There is also an evolution of the Au average coordination number with light atoms, which decreases from 3 to about 2.4, indicating that during this stage, Au(III) continues its reduction to Au(I). The UV−vis spectrophotometric results and the EXAFS measurements indicate that there is still no evident reduction to Au(0) at this stage. As previously discussed in the literature, this fact could be explained considering that, even with very favorable reducing potentials for the reduction of Au(I) to Au(0), the presence of organic medium can decrease the rate of electron transfer between Au(I) and the reducing agent. Hence, the reduction of the Au(I) complex will be kinetically limited.[33] Hence, in this stage, an evolution to longer objects formed by Au(I) complexes (still in the absence of metallic gold) can be postulated.

4.3. Stage 3: 160−270 min of Reaction. After 160 min of reaction, the first signals of reduction from Au(I) to Au(0) are observed. The UV−vis spectra show an increase in the absorbance at 490 nm, starting at about 150−160 min, that points to the beginning of formation of metallic entities of very low diameters (Figure 2). This band at 490 nm is associated with quantized transitions, as expected for metallic structures of very low dimensions.[25] These results can be considered incompatible, in principle, with the EXAFS results (Figure 9b) that do not show the appearance of an Au−Au coordination shell (at a distance compatible with metallic species) until 270 min. However, it is important to recall that the EXAFS Au−Au coordination number is weighted by both the size of the metallic particles and the fraction of the Au atoms forming them.[34] Hence, when the first metallic seeds appear, the Au−Au average coordination number is too small to be detected by EXAFS. For this reason, clear EXAFS evidences of the presence of an Au−Au coordination number are only observed after the size and fraction of gold in the metallic particles had grown significantly.

At 160 min, SAXS measurements show a decrease in the diameter of the objects from 2.6 nm to about 1.6 nm. This decrease in the diameter of the objects would indicate that Au reduction takes place by simultaneous electronic transfer and expulsion of ligands from the inside of the aggregates to the surrounding medium. Length of the disk-like objects also increases abruptly at this point (Figure 5b). After this process starts, simultaneous presence of Au(0) and Au(I) species are observed, demonstrating that reduction from Au(I) to Au(0) is a slow process that probably requires the concerted presence of several Au(I) units to take place. In this stage, TEM images also evidence the presence of crystalline wire-like metallic structures, still along with some diffused objects assigned to not-reduced precursors. Hence, this stage starts with the reduction of Au(I) complexes to give the first Au(0) structures. Apparently, this process would be initiated after the formation of aggregates that would be acting as seeds for the further reduction to metallic gold, as shown from the SAXS results.

4.4. Stage 4: 270−480 min of Reaction. A constant increase in the Au−Au coordination number is observed from 270 min on, reaching a value of almost 7 at 480 min (Figure 9b). In the same process, the coordination number with light atoms decreases continuously to reach a value of 1.3 at 480 min, indicating a high progress in the reduction from Au(I) to Au(0), resulting in the growth of the NWs. Appearance of first SAXS correlation peaks takes place at 270 min, when metallic structures start to be evident by EXAFS. These features can be assigned to the formation of an hexagonal arrangement of Au(0) NWs with a value of the lattice parameter of about 9.0 nm (Figure S3, Supporting Information). This value is related to the distance between nanowires in the hexagonal arrangement. By subtracting the diameter of the wires with the lattice parameter (9.0 and 1.7 nm, respectively), separation between nanostructures can be calculated as 7.3 nm. This value agrees with the previous reports showing that, in solution, a bilayer of OAm molecules is formed between wires (the OAm length in all-trans configuration is about 2.1 nm).[16,35] Nouh et al.[35] have shown that the distance between NWs in these ordered structures changes with the concentration of OAm present in the solution (and also with the type of ligand), which explains the differences found in the literature between lattice parameters for the same arrangement measured in situ or ex situ. They also showed the presence of the oleylammonium group at the bilayer (by ^{1}H NMR), indicating that the coordinating group at the gold surface is the chloride ion. The TEM images show the presence of bundles of NWs separated by a constant distance, although this separation cannot be compared with that found in the solution due to changes produced during the evaporation of the solvent.

4.5. Stage 5: 480−600 min of Reaction. In this final stage of the reaction, EXAFS results show that the average Au−Au coordination number continues to grow at a lower speed until reaching its final value of 8.5. The expected coordination number for NWs with 1.7 nm of diameter would be close to 10. Failure to reach this expected value could probably indicate that a part of the gold remains unreduced. The EXAFS results obtained after 20 h of synthesis show a slight increase in the Au−Au coordination number, indicating

DOI: 10.1021/acs.jpcc.8b10449
J. Phys. Chem. C 2018, 122, 29051−29061

that a slow reduction of the remaining Au(I) could still be taking place. The remaining coordination number with light elements fitted at the end of the reaction may be associated with both unreacted Au(I) and OAm molecules acting as capping of the NWs. This is consistent with the SAXS results and previous studies[16,35] showing that Au NWs are coated with an oleylamine/oleylammonium layer.

5. CONCLUSIONS

We performed a combined in situ characterization through X-ray absorption spectroscopy (XANES and EXAFS) and small-angle X-ray scattering (SAXS), along the complete synthesis reaction of Au nanowires in hexane solution. We found that the reaction can be divided into five stages. At the beginning, Au(III) atoms form complexes with planar-square geometry. Gold is then continuously reduced from Au(III) to Au(I), regardless of TIPS addition, forming disk-like structures with a diameter of about 2.6 nm and a thickness of about 0.3−0.5 nm by the aggregation of Au(I) and/or Au(III) complexes. Characteristic length/thickness of disk-like objects increase for longer times of reaction presumably through interaction between Au(I) centers via aurophilic interactions, which result in the stacking of the disks to form cylinders of longer length. After 160 min, most of the Au(III) has been reduced to Au(I) and the reduction to Au(0) starts. The diameter of the objects is reduced from 2.6 nm to about 1.6 nm and a continuous increase in the length is seen, indicating the formation of the nanowires, which form an hexagonal arrangement separated by a bilayer of OAm molecules. The length of the NWs continues to grow while Au(I) is slowly reduced to Au(0) in a process that takes more than 10 h to finish. Bundles of Au NWs with lengths of several microns are the final product of the reaction.

Our results provide new evidence regarding the mechanism of formation and growth of Au NWs and the Au atoms reduction pathway, including the nature and shape of the initial structures that act as seeds for the anisotropic growth of the wires.

■ ASSOCIATED CONTENT

Supporting Information

The Supporting Information is available free of charge on the ACS Publications website at DOI: 10.1021/acs.jpcc.8b10449.

Details of SAXS analysis and modeling; AFM images and analysis; XANES analysis; complete results of the EXAFS fits (PDF)

■ AUTHOR INFORMATION

Corresponding Authors

*E-mail: hoppe@fi.mdp.edu.ar. Tel: +54-223-4816600 (C.E.H.).

*E-mail: ramallo@inifta.unlp.edu.ar. Tel: +54-221-4257291 (R.L.).

ORCID

Fernando Pschunder: 0000-0003-1196-6524

Julieta Puig: 0000-0002-4442-2286

Lisandro J. Giovanetti: 0000-0001-5286-3463

Cristián Huck-Iriart: 0000-0001-5734-2499

Félix G. Requejo: 0000-0003-4439-864X

David Buceta: 0000-0002-3297-6695

Cristina E. Hoppe: 0000-0002-4352-4467

José M. Ramallo-López: 0000-0002-8233-2644

Notes

The authors declare no competing financial interest.

■ ACKNOWLEDGMENTS

This work was financially supported by ANPCyT (PICT 2015-2285 and PICT 2015-1433), CONICET (PIP No. 0594), UNMdP and UNLP (Project 11/X790) from Argentina. Partial support by Laboratório Nacional de Luz Síncrotron (LNLS), Brazil under proposal 20160225 is acknowledged. D.B. expresses gratitude for a postdoctoral grant from Xunta de Galicia, Spain (POS-A/2013/018). We acknowledge Dr. Eduardo D. Pietro for his assistance with the AFM imaging and analysis.

■ REFERENCES

(1) Halder, A.; Ravishankar, N. Ultrafine Single-Crystalline Gold Nanowire Arrays by Oriented Attachment. *Adv. Mater.* **2007**, *19*, 1854−1858.

(2) Lu, X.; Yavuz, M. S.; Tuan, H.-Y.; Korgel, B. A.; Xia, Y. Ultrathin Gold Nanowires Can Be Obtained by Reducing Polymeric Strands of Oleylamine−AuCl Complexes Formed via Aurophilic Interaction. *J. Am. Chem. Soc.* **2008**, *130*, 8900−8901.

(3) Li, Z.; Tao, J.; Lu, X.; Zhu, Y.; Xia, Y. Facile Synthesis of Ultrathin Au Nanorods by Aging the AuCl(Oleylamine) Complex with Amorphous Fe Nanoparticles in Chloroform. *Nano Lett.* **2008**, *8*, 3052−3055.

(4) Huo, Z.; Tsung, C.; Huang, W.; Zhang, X.; Yang, P. Sub-Two Nanometer Single Crystal Au Nanowires. *Nano Lett.* **2008**, *8*, 2041−2044.

(5) Wang, C.; Hu, Y.; Lieber, C. M.; Sun, S. Ultrathin Au Nanowires and Their Transport Properties. *J. Am. Chem. Soc.* **2008**, *130*, 8902−8903.

(6) Pazos-Pérez, N.; Baranov, D.; Irsen, S.; Hilgendorff, M.; Liz-Marzán, L. M.; Giersig, M. Synthesis of Flexible, Ultrathin Gold Nanowires in Organic Media. *Langmuir* **2008**, *24*, 9855−9860.

(7) Cui, H.; Hong, C.; Ying, A.; Yang, X.; Ren, S. Ultrathin Gold Nanowire-Functionalized Carbon Nanotubes for Hybrid Molecular Sensing. *ACS Nano* **2013**, *7*, 7805−7811.

(8) Kisner, A.; Heggen, M.; Mayer, D.; Simon, U.; Offenhäusser, A.; Mourzina, Y. Probing the Effect of Surface Chemistry on the Electrical Properties of Ultrathin Gold Nanowire Sensors. *Nanoscale* **2014**, *6*, 5146−5155.

(9) Yang, L.; Zhang, Y.; Chu, M.; Deng, W.; Tan, Y.; Ma, M.; Su, X.; Xie, Q.; Yao, S. Facile Fabrication of Network Film Electrodes with Ultrathin Au Nanowires for Nonenzymatic Glucose Sensing and Glucose/O2 Fuel Cell. *Biosens. Bioelectron.* **2014**, *52*, 105−110.

(10) Xu, J.; Wang, H.; Liu, C.; Yang, Y.; Chen, T.; Wang, Y.; Wang, F.; Liu, X.; Xing, B.; Chen, H. Mechanical Nanosprings: Induced Coiling and Uncoiling of Ultrathin Au Nanowires. *J. Am. Chem. Soc.* **2010**, *132*, 11920−11922.

(11) Xu, J.; Jiang, W. Confinement of Polymer-Tethered Gold Nanowires in Polymeric Colloids. *Macromolecules* **2014**, *47*, 2396−2403.

(12) Chen, Y.; Ouyang, Z.; Gu, M.; Cheng, W. Mechanically Strong, Optically Transparent, Giant Metal Superlattice Nanomembranes From Ultrathin Gold Nanowires. *Adv. Mater.* **2013**, *25*, 80−85.

(13) Sánchez-Iglesias, A.; Rivas-Murias, B.; Grzelczak, M.; Pérez-Juste, J.; Liz-Marzán, L. M.; Rivadulla, F.; Correa-Duarte, M. A. Highly Transparent and Conductive Films of Densely Aligned Ultrathin Au Nanowire Monolayers. *Nano Lett.* **2012**, *12*, 6066−6070.

(14) Huo, Z.; Tsung, C.; Huang, W.; Zhang, X.; Yang, P. Sub-Two Nanometer Single Crystal Au Nanowires. *Nano Lett.* **2008**, *8*, 2041−2044.

(15) Feng, H.; Yang, Y.; You, Y.; Li, G.; Guo, J.; Yu, T.; Shen, Z.; Wu, T.; Xing, B. Simple and Rapid Synthesis of Ultrathin Gold Nanowires, Their Self-Assembly and Application in Surface-Enhanced Raman Scattering. *Chem. Commun.* **2009**, *No. 15*, 1984−1986.

(16) Loubat, A.; Impéror-Clerc, M.; Pansu, B.; Meneau, F.; Raquet, B.; Viau, G.; Lacroix, L.-M. Growth and Self-Assembly of Ultrathin Au Nanowires into Expanded Hexagonal Superlattice Studied by in Situ SAXS. *Langmuir* **2014**, *30*, 4005−4012.
(17) Loubat, A.; Lacroix, L.-M.; Robert, A.; Impéror-Clerc, M.; Poteau, R.; Maron, L.; Arenal, R.; Pansu, B.; Viau, G. Ultrathin Gold Nanowires: Soft-Templating versus Liquid Phase Synthesis, a Quantitative Study. *J. Phys. Chem. C* **2015**, *119*, 4422−4430.
(18) Halder, A.; Ravishankar, N. Gold Nanostructures from Cube-Shaped Crystalline Intermediates. *J. Phys. Chem. B* **2006**, *110*, 6595−6600.
(19) Ristau, R.; Tiruvalam, R.; Clasen, P. L.; Gorskowski, E. P.; Harmer, M. P.; Kiely, C. J.; Hussain, I.; Brust, M. Electron Microscopy Studies of the Thermal Stability of Gold Nanoparticle Arrays. *Gold Bull.* **2009**, *42*, 133−143.
(20) Corthey, G.; Giovanetti, L. J.; Ramallo-López, J. M.; Zelaya, E.; Rubert, A. A.; Benitez, G. A.; Requejo, F. G.; Fonticelli, M. H.; Salvarezza, R. C. Synthesis and Characterization of Gold@Gold(I)−Thiomalate Core@Shell Nanoparticles. *ACS Nano* **2010**, *4*, 3413−3421.
(21) Laiho, T.; Leiro, J.; Lukkari, J. XPS Study of Irradiation Damage and Different Metal−Sulfur Bonds in Dodecanethiol Monolayers on Gold and Platinum Surfaces. *Appl. Surf. Sci.* **2003**, *212−213*, 525−529.
(22) Ramallo-López, J. M.; Giovanetti, L. J.; Vicentin, F. C.; Requejo, F. G. XANES Study of the Radiation Damage on Alkanethiolates-Capped Au Nanoparticles. *J. Phys. Conf. Ser.* **2013**, *430*, No. 012034.
(23) Ravel, B.; Newville, M. ATHENA, ARTEMIS, HEPHAESTUS: Data Analysis for X-Ray Absorption Spectroscopy Using IFEFFIT. *J. Synchrotron Radiat.* **2005**, *12*, 537−541.
(24) Zabinsky, S. I.; Rehr, J. J.; Ankudinov, A.; Albers, R. C.; Eller, M. J. Multiple-Scattering Calculations of x-Ray-Absorption Spectra. *Phys. Rev. B* **1995**, *52*, 2995−3009.
(25) Takahata, R.; Yamazoe, S.; Koyasu, K.; Tsukuda, T. Surface Plasmon Resonance in Gold Ultrathin Nanorods and Nanowires. *J. Am. Chem. Soc.* **2014**, *136*, 8489−8491.
(26) Yu, Y.; Cui, F.; Sun, J.; Yang, P. Atomic Structure of Ultrathin Gold Nanowires. *Nano Lett.* **2016**, *16*, 3078−3084.
(27) Svergun, D. I. Determination of the Regularization Parameter in Indirect-Transform Methods Using Perceptual Criteria. *J. Appl. Crystallogr.* **1992**, *25*, 495−503.
(28) Cotton, F. A.; Wilkinson, G. *Advanced Inorganic Chemistry: A Comprehensive Text*, 3rd ed.; Interscience Publishers: New York, 1972.
(29) Zhang, P.; Sham, T. K. X-Ray Studies of the Structure and Electronic Behavior of Alkanethiolate-Capped Gold Nanoparticles: The Interplay of Size and Surface Effects. *Phys. Rev. Lett.* **2003**, *90*, No. 245502.
(30) Lu, X.; Tuan, H.-Y.; Korgel, B. A.; Xia, Y. Facile Synthesis of Gold Nanoparticles with Narrow Size Distribution by Using AuCl or AuBr as the Precursor. *Chem. - Eur. J.* **2008**, *14*, 1584−1591.
(31) Schmidbaur, H.; Schier, A. Aurophilic Interactions as a Subject of Current Research: An up-Date. *Chem. Soc. Rev.* **2012**, *41*, 370−412.
(32) Metrangolo, P.; Meyer, F.; Pilati, T.; Resnati, G.; Terraneo, G. Halogen Bonding in Supramolecular Chemistry. *Angew. Chem., Int. Ed.* **2008**, *47*, 6114−6127.
(33) Kisner, A. *Ultrathin Gold Nanowires: Chemistry, Electrical Characterization and Application to Sense Cellular Biology*; Schriften des Forschungszentrums Jülich Reihe Information; Forschungszentrum Jülich: Jülich, 2012.
(34) Frenkel, A. I.; Yevick, A.; Cooper, C.; Vasic, R. Modeling the Structure and Composition of Nanoparticles by Extended X-Ray Absorption Fine-Structure Spectroscopy. *Annu. Rev. Anal. Chem.* **2011**, *4*, 23−39.
(35) Nouh, E. S. A.; Baquero, E. A.; Lacroix, L.-M.; Delpech, F.; Poteau, R.; Viau, G. Surface-Engineering of Ultrathin Gold Nanowires: Tailored Self-Assembly and Enhanced Stability. *Langmuir* **2017**, *33*, 5456−5463.

DOI: 10.1021/acs.jpcc.8b10449
J. Phys. Chem. C 2018, 122, 29051−29061